Title

Microscopic Study of Atomic Layer Deposition of TiO2 on GaAs and Its Photocatalytic Application

Journal

Chemistry of Materials, 27(23)

ISSN

0897-4756

Authors

Qiu, Jing
Zeng, Guangtong
Ha, Mai-Anh
et al.

Publication Date

2015-12-08

DOI

10.1021/acs.chemmater.5b03246

Peer reviewed

CHEMISTRY OF MATERIALS

Article

pubs.acs.org/cm

Microscopic Study of Atomic Layer Deposition of TiO_2 on GaAs and Its Photocatalytic Application

Jing Qiu,[†] Guangtong Zeng,[§] Mai-Anh Ha,[∥] Bingya Hou,[‡] Matthew Mecklenburg,[¶] Haotian Shi,[§] Anastassia N. Alexandrova,[∥,⊥] and Stephen B. Cronin*[,‡,§]

[†]Department of Materials Science, [‡]Department of Electrical Engineering, [§]Department of Chemistry, and [¶]Center for Electron Microscopy and Microanalysis, University of Southern California, Los Angeles, California 90089, United States

[∥]Department of Chemistry and Biochemistry and [⊥]California NanoSystems Institute, University of California Los Angeles, Los Angeles, California 90025, United States

Supporting Information

ABSTRACT: We report a microscopic study of *p*-GaAs/TiO_2 heterojunctions using cross-sectional high resolution transmission electron microscopy (HRTEM). The photocatalytic performance for both H_2 evolution and CO_2 reduction of these heterostructures shows a very strong dependence on the thickness of the TiO_2 over the range of 0−15 nm. Thinner films (1−10 nm) are amorphous and show enhanced catalytic performance with respect to bare GaAs. HRTEM images and electron energy loss spectroscopy (EELS) maps show that the native oxide of GaAs is removed by the $TiCl_4$ atomic layer deposition (ALD) precursor, which is corrosive. Ti^{3+} defect states (i.e., O vacancies) in the TiO_2 film provide catalytically active sites, which improve the photocatalytic efficiency. Density functional theory (DFT) calculations show that water molecules and CO_2 molecules bind stably to these Ti^{3+} states. Thicker TiO_2 films (15 nm) are crystalline and have poor charge transfer due to their insulating nature, while thinner amorphous TiO_2 films are conducting.

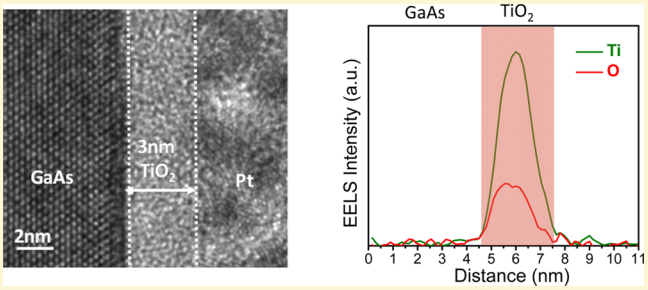

Since Fujishima and Honda initially demonstrated photocatalytic water splitting using TiO_2 in 1972,[1] the study of photocatalysis has received worldwide interest due to its potential applications in solar fuel generation either through water splitting or CO_2 reduction. While TiO_2 is a widely studied material, its theoretical photocurrent density under one-sun illumination is only about 1−2 mA/cm^2. Narrower band gap materials like Si, InP, and GaAs are more promising candidates, since their theoretical photocurrent densities are 44, 35, and 32 mA/cm^2, respectively.[2] However, one of the primary problems, which prevents these narrower band gap materials from being utilized as photocatalysts, is that their surfaces are not photochemically stable.[3] Therefore, passivating their surfaces to protect them from photocorrosion without sacrificing their photoconversion efficiency will enable more efficient photocatalytic systems to be developed.

Recently, several groups have demonstrated that a very thin layer of TiO_2 can be used to make these narrower band gap materials stable. Chen et al. first showed that TiO_2 deposited by atomic layer deposition (ALD) can stabilize silicon photoanodes for water oxidation.[4] Hu et al. also reported that amorphous TiO_2 coatings stabilize Si, GaAs, and GaP photoanodes for efficient water oxidation.[5] For the study of photocathodes, it is also reported that TiO_2 can be used to protect *p*-InP from corrosion and provide efficient solar-driven H_2 production.[6,7] Our group's previous work showed that, in addition to making GaP and InP photocathodes photochemically stable, a thin layer of TiO_2 can also provide substantial enhancement in the photoconversion efficiency for both H_2 evolution and CO_2 reduction.[8−10] More recently, Lin et al. has also discussed similar enhancement in photocatalytic H_2 evolution using InP and TiO_2 films deposited with various ALD precursors, including TDMAT (i.e., $[(CH_3)_2N]_4Ti$) and titanium isopropoxide (i.e., $C_{12}H_{28}O_4Ti$).[11] While these previous works are very encouraging, a detailed microscopic picture of these TiO_2-passivated heterostructures is lacking.

In this report, we provide a detailed study of TiO_2 layer growth on GaAs by atomic layer deposition using high resolution transmission electron microscopy (HRTEM) and electron energy-loss spectroscopy (EELS), as well as plane wave density functional theory (PW-DFT) calculations, which are carried out to provide a detailed picture of the *p*-GaAs/TiO_2 interface and explore the role of surface binding of reactants and intermediate species to the TiO_2 surface. In this work, *p*-type (111) oriented GaAs substrates with a Zn dopant concentration of 6×10^{16}cm^{-3} (obtained from University Wafer, Inc.) are used as the photocathode. There is approximately 3 nm of native oxide on the GaAs surface

Received: August 20, 2015
Revised: November 17, 2015
Published: November 17, 2015

DOI: 10.1021/acs.chemmater.5b03246
Chem. Mater. 2015, 27, 7977−7981

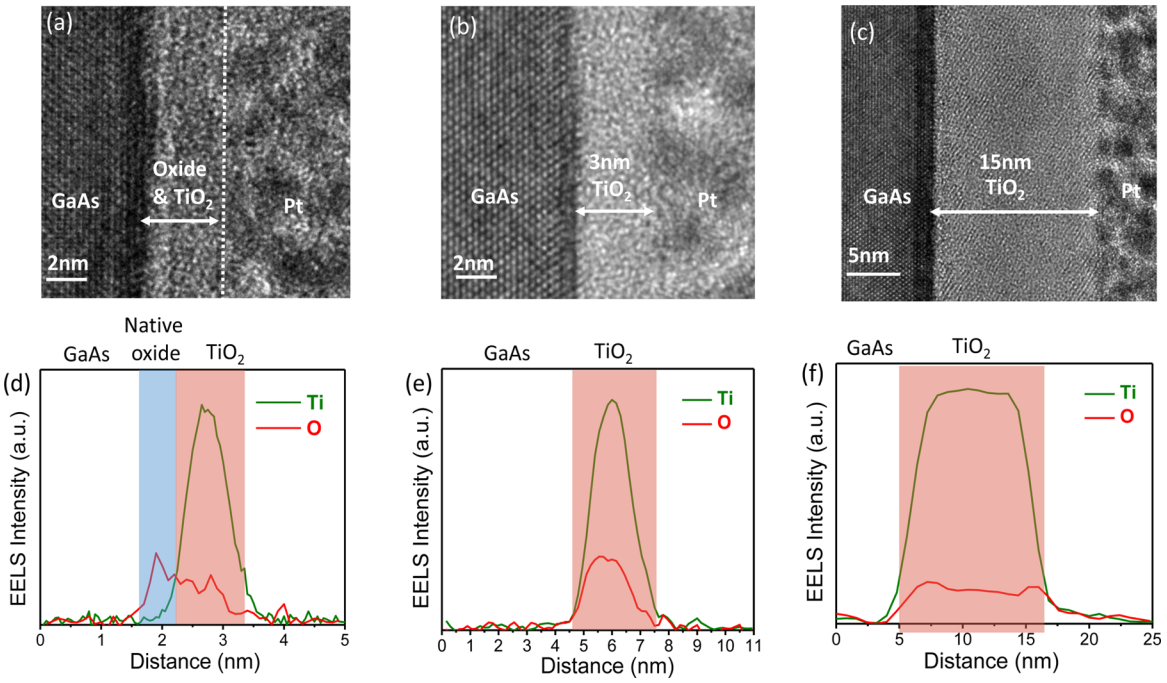

Figure 1. High resolution TEM image of TiO_2 films deposited with (a) 25 cycles, (b) 75 cycles, and (c) 500 cycles of atomic layer deposition on GaAs. Note that, for TEM sample preparation and imaging purposes, the surface of the substrate is coated with a thick layer of Pt. (d,e) EELS spatial profiles of Ti L edge (green line) and O K edge map (red line) for the 25, 75, and 500 cycle TiO_2 on GaAs samples, respectively.

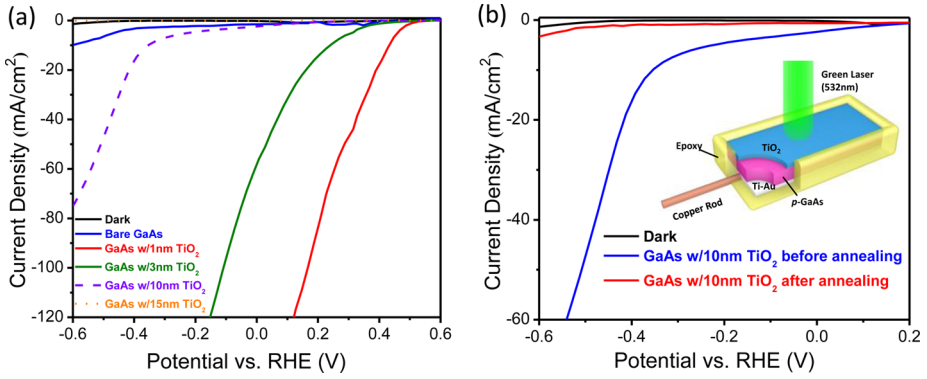

Figure 2. Photocatalytic water splitting current−potential curves for samples of (a) GaAs photocatalysts with various thicknesses of TiO_2 and (b) GaAs with 10 nm TiO_2 before and after annealing under 532 nm illumination in a 0.5 M H_2SO_4 pH = 0 solution. The dark curves are for bare GaAs. Inset shows schematic diagram of the GaAs/TiO_2 sample geometry.

(Figure S1). Atomic layer deposition of TiO_2 was performed at 250 °C on the *p*-GaAs wafers using $TiCl_4$ as the titanium source and water vapor as the oxygen source. $TiCl_4$ is used for the first half-cycle, and argon was the carrier gas with a flow rate of 20 sccm during deposition. Figure 1a−c shows HRTEM images of TiO_2 films deposited with 25, 75, and 500 cycles of atomic layer deposition on GaAs. These films have nominal thicknesses of 1, 3, and 15 nm, respectively. Pt was deposited in order to enable cross section sample preparation using focused ion beam milling and was not used in the photocatalysis measurements described below. Figure 1d−f shows EELS spatial profiles of the Ti and O species for the 25, 75, and 500 cycle TiO_2 on GaAs samples, respectively. In Figure 1d, the oxygen signal increases approximately 0.5 nm before the Ti signal, indicating the presence of the GaAs native oxide underneath the TiO_2 layer. Therefore, on the basis of these EELS spectra, there is both native GaAs oxide and amorphous TiO_2 on the GaAs surface after the 25 cycle ALD process. It should be noted that the thickness of GaAs's native oxide is substantially lower than the 3 nm native oxide observed on bare GaAs (without TiO_2 deposition), as shown in the inset diagram in Figure 2b. After 25 ALD cycles, the native oxide of the GaAs was partially removed due to the Cl^- ions from the $TiCl_4$ precursor. Figure 1e shows the EELS spatial maps of GaAs with 75 cycles of atomic layer deposition of TiO_2. Here, both the O and Ti signals increase together, indicating that the native oxide of GaAs has been completely removed during the ALD process. With further growth of 500 cycles, the amorphous TiO_2 becomes crystalline as shown in Figure 1f. This layer of TiO_2 is in the anatase phase with clear lattice planes along the 101 direction, identified by the interplane distance of 3.5 ± 0.1 Å, as indicated in Figure S2. Shi et al.'s work also shows anatase phase TiO_2 formed by high temperature atomic layer deposition.[12]

Figure 2a shows the H_2 evolution photocurrent−voltage curves of *p*-GaAs photocathodes with various thicknesses of

DOI: 10.1021/acs.chemmater.5b03246
Chem. Mater. 2015, 27, 7977−7981

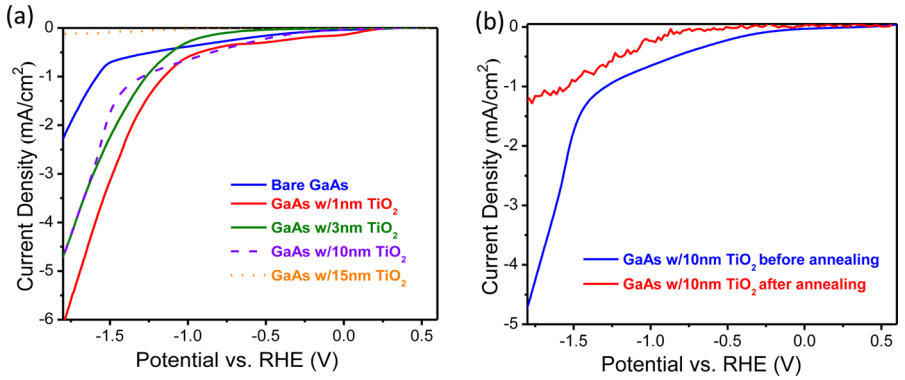

Figure 3. Photocatalytic CO_2 reduction current−potential curves for samples of (a) GaAs photocatalysts with various thicknesses of TiO_2 and (b) GaAs with 10 nm TiO_2 before and after annealing under 532 nm illumination in a 0.02 M $[EMIM]BF_4$ nonaqueous CO_2 saturated electrolyte.

TiO_2 under 910 mW/cm^2 532 nm illumination in a 0.5 M H_2SO_4 electrolyte, plotted together with bare GaAs. The bare GaAs (blue curve) exhibits an onset of photocurrent at a potential of approximately −0.05 V vs RHE. The TiO_2-passivated GaAs shows a clear shift in the onset potential. The sample with a nominal thickness of 1 nm TiO_2 exhibits the most prominent shift, lowering the overpotential from −0.75 V (blue curve) to 0.32 V (at 10 mA/cm^2) (red curve) with a 120×-fold enhancement of photocurrent over bare GaAs at 0 V vs RHE. This potentials shifts can be seen more clearly from the log−linear plot of the photo-I−V data shown in Figure S7. These results were reproduced consistently in several different sets of samples. The enhancement is attributed to the oxygen vacancies (Ti^{3+} states), which provide the photocatalytically active site for H_2 evolution, which is consistent with the results from PW-DFT calculations shown in Figure 4b. At the same time, we observe no improvement when the TiO_2 thickness reaches 15 nm, as shown by the orange curve. This is because amorphous TiO_2 is far more conductive than crystalline TiO_2, which is insulating and, therefore, impedes charge transfer to the ions in solution. In the works of Chen et al.[4] and Viswanathan et al.,[13] it was assumed that electrons were tunneling through a high-quality ALD layer,[13] whereas in the work of Hu et al.,[5] it was reported that electronically leaky amorphous TiO_2 films enabled efficiency charge transport to the ions in solution. Since then, detailed DFT calculations have established the conduction mechanism in amorphous TiO_2 films.[14] For TiO_2 thicknesses between 1 and 15 nm, the photocatalytic performance becomes substantially worse with increasing thickness. We believe the TiO_2 films become increasingly crystalline, and hence more insulating, as the thickness is increased. Figure 2b shows the photocurrent−voltage curves for 10 nm TiO_2 on GaAs before and after annealing. The photocurrent decreases dramatically after annealing, due to the crystallization of the TiO_2 during annealing, which is consistent with the result of the 15 nm crystalline TiO_2 film on GaAs. We also measured the photo-I−V characteristics of both etched and unetched bare GaAs (Figure S6). There is not much difference in the photo-I−V characteristics, which indicate that native oxide has a limited effect on the H_2 evolution reaction. The H_2 product was detected using gas chromatography, as shown in Figure S3a.

In addition to H_2 evolution, we also characterized the photocatalytic performance of these p-GaAs/TiO_2 heterostructures for CO_2 reduction to CO. A nonaqueous ionic liquid electrolyte was used to exclude the effect of H_2O splitting, which has a lower onset potential than CO_2 reduction and tends to dominate the Faradaic efficiency. Figure 3a shows the photocurrent−voltage curves for GaAs passivated with various thicknesses of TiO_2 measured in an AcN electrolyte with 0.02 M $[EMIM]BF_4$ under 532 nm wavelength illumination. During these measurements, CO_2 is continuously bubbled through the solution. For TiO_2 thicknesses up to 10 nm, TiO_2-passivated GaAs samples exhibit a higher photocurrent than bare GaAs (blue curve). Also, clear shifts in the onset potential required to initiate this reaction can also be seen in the I−V characteristics of samples passivated with TiO_2, which is consistent with the predictions of the PW-DFT calculations discussed below. Again, we observed no improvement when the TiO_2 thickness reaches 15 nm, as shown in the orange curve, due to its insulating crystalline nature. Figure 3b shows the photocurrent−voltage curves for 10 nm TiO_2 on GaAs before and after annealing. The photocurrent decreases dramatically after annealing, which is due to the crystallization of TiO_2 during annealing. Photocatalytic production of CO from CO_2 reduction was analyzed using gas chromatography, as shown in Figure S3b.

It is widely accepted that the reduction of H_2O to form H_2 occurs predominantly at the Ti^{3+}-O vacancy sites due to the reaction of adsorbed H^+ ions.[15,16] Thus, a higher concentration of O vacancies correspond to more active sites, resulting in a higher hydrogen generation efficiency. Similarly, these Ti^{3+}-O vacancy sites can also provide the catalytically active sites for CO_2 reduction.[17−19] As was previously done,[20] plane wave density functional theory (PW-DFT) calculations were performed on a supercell of anatase composed of 16 TiO_2 units exposing the 101 surface. The Quantum Espresso package was used with the most recently available ultrasoft pseudopotentials with scalar relativistic corrections,[21−24] and spin-unrestricted calculations were done employing the Perdew−Burke−Ernzerhof (PBE) functional.[25] Kinetic energy cutoffs of 435.2 (4.352) eV were applied to the wave functions (charge density) with a 1 × 1 × 1 Monkhorst-Pack k-point grid centered at Γ. A DFT+D+U approach was instituted with Grimme's method[26] for dispersion forces (+D) and a Hubbard U parameter of 3.6 eV (+U). An explanation for this approach was provided in our previous study.[20] Clean, stoichiometric anatase and defective anatase with a surface oxygen vacancy were both investigated in this study. Adsorption energies were calculated by subtracting energies of the two components (H_2O and surface) from the energy of the adsorbed system:

$$E_{ads} = E[\text{surf} + H_2O] - E[\text{surf}] - E[H_2O]$$

DOI: 10.1021/acs.chemmater.5b03246
Chem. Mater. 2015, 27, 7977−7981

where the surface was stoichiometric anatase or defective anatase with a surface oxygen vacancy.

A manual search was performed to determine the global minimum of adsorbed H_2O to the anatase support reproducing the same geometries found in Tilocca et al.'s study on water on anatase.[27] Adsorption energies were favorable between neutral H_2O adsorbed to stoichiometric (−1.26 eV as indicated in Figure S5) and defective anatase (−1.50 eV). These energies differ from those of Tilocca et al. due to possible interactions across our smaller supercell and the additional consideration of dispersion forces, which lowered the adsorption to stoichiometric anatase significantly (Tilocca et al. reported −0.74 eV) and to defective anatase minimally (Tilocca et al. reported −1.48 eV). As in our findings with CO_2, molecules adsorbed to defective anatase tend to fill the surface oxygen vacancy. In Figure 4b, the water molecule attempts to both fill the oxygen

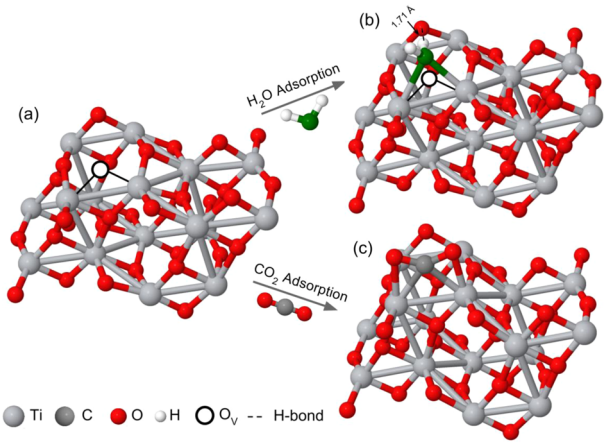

Figure 4. PW-DFT calculated structure for anatase TiO_2 with O vacancies (a) before adsorption, (b) after H_2O adsorption and relaxation, and (c) after CO_2 adsorption and relaxation.

vacancy with its oxygen (colored green) and retain a hydrogen bond to the neighboring surface oxygen on the oxide support. Moreover, the hydrogen bond might be considered an "activated" bond with a length of 1.71 Å as compared to 1.89 Å on the stoichiometric support, indicating that the system is approaching the proton transfer to the O atom of the support. In a molecular dynamics study, Tilocca et al. estimated the activation barrier from adsorption of H_2O to dissociation of the H_2O to two hydroxyls to be ∼0.1 eV.[28] Moreover, Fujimori et al. maintained that hydroxylation of their MgO support provided the pathway for two mechanisms of hydrogen evolution: the direct redox process and the water−gas shift reaction in the presence of CO.[29] This indicates that Ti^{3+}-O sites are more energetically favorable for H_2O adsorption, which results in higher H_2 evolution efficiencies, consistent with previous reports in the literature.[16] This calculation combined with our previous finding[20] of spontaneous CO_2 reduction on defective anatase (a charge transfer of 0.897 *e* from the support to CO_2) indicates that the O vacancies provide catalytically active sites for CO_2 and H_2O absorption, and no overpotential is required to form the CO_2^- intermediate.

In conclusion, we have carried out a microscopic study of GaAs photocathodes passivated with various thicknesses of TiO_2 using atomic layer deposition. High resolution transmission electron microscopy (HRTEM) and electron energy-loss spectroscopy (EELS) show that the native oxide of GaAs is removed by the $TiCl_4$ precursor during the TiO_2 growth. The photocatalytic performance for both H_2 evolution and CO_2 reduction of these heterostructures shows a very strong dependence on the thickness of the TiO_2 over the range of 0−15 nm. Thinner TiO_2 films are amorphous and show enhanced catalytic performance with respect to bare GaAs, whereas thicker TiO_2 films (15 nm) are single crystal and have poor charge transfer due to the insulating nature of crystalline TiO_2. DFT calculations show that the water and CO_2 molecules bind stably to TiO_2, which can further improve the photocatalytic charge transfer process.

EXPERIMENTAL METHODS

Ohmic back contacts were made for the *p*-GaAs by evaporating 5 nm of Ti followed by 50 nm of Au. The Ti−Au film was then connected to the external circuitry with a copper wire and coated with epoxy cement to insulate it from the electrolytic solution, as illustrated in the inset diagram in Figure 2b. High resolution transmission electron microscope images of TiO_2 on GaAs were taken with a JEOL JEM-2100F TEM equipped with a Gatan Quantum SE GIF quantum energy filter. A layer of Pt was deposited on the surfaces of samples as part of the cross section sample preparation using standard focused ion beam sample preparation techniques. TiO_2 films were annealed in a furnace at 450 °C for 30 min while flowing N_2 gas. The photocatalytic H_2 evolution measurements were carried out in a pH = 0 solution of 0.5 M H_2SO_4 using a three-terminal potentiostat with the prepared samples, a Ag/AgCl electrode, and a graphite electrode functioning as the working, reference, and counter electrodes, respectively. The area of the exposed electrode surface is about 0.1 cm^2. A 532 nm continuous-wave laser was used to excite the samples, and low to moderate power excitation (910 mW/cm^2) was used to avoid optical heating. The nonaqueous solution (for CO_2 reduction) was prepared using acetonitrile (AcN, 99.99%), dimethyl sulfoxide (DMSO, 99.96% D, Sigma-Aldrich), and 1-ethyl-3-methylimidazolium tetrafluoroborate ($[EMIM]BF_4$, 99.0%, HPLC, Sigma-Aldrich). An anion exchange membrane (Selemion AMV, Anion Exchange Membrane, AGC Inc.) was used to separate the working and counter electrodes to prevent oxidation of the reduced CO_2 products. This anion exchange membrane only allows negative ions to transfer through the membrane, which prevents the oxylate intermediate from participating in the oxygen evolution half-reaction at the counter electrode. A three-terminal potentiostat was used with the prepared semiconductor samples as the working electrode, a $Ag/AgNO_3$ reference electrode, and a Pt wire as the counter electrode. The $Ag/AgNO_3$ electrode was made of a silver wire immersed in 0.01 M silver nitrate dissolved in 0.1 M TEAP/AcN. Also, the reference electrode was calibrated against a ferrocene/ferrocenium (Fc^+/Fc) redox couple to confirm that it gave the right potential with respect to NHE. A detailed discussion of the calibration can be found in our previous work.[10] Before each measurement, CO_2 was purged through the solution on the working electrode side for 30 min. H_2 evolution and the gaseous products from the CO_2 reduction reaction were analyzed with a gas chromatograph (GC) (Bruker GC-450) equipped with a thermal conductivity detector (TCD) and a carbon-plot column (Agilent). The produced CO was quantified by integrating the area of the CO peak, and this was related to the calibration data (Figure S4).

ASSOCIATED CONTENT

Supporting Information

The Supporting Information is available free of charge on the ACS Publications website at DOI: 10.1021/acs.chemmater.5b03246.

TEM images of bare GaAs and 10 nm TiO_2 on GaAs, gas chromatography data for product after reaction, schematic diagram of H_2O adsorption on stoichiometric anatase, and additional photocatalytic current−potential curves. (PDF)

DOI: 10.1021/acs.chemmater.5b03246
Chem. Mater. 2015, 27, 7977−7981

AUTHOR INFORMATION

Notes

The authors declare no competing financial interest.

ACKNOWLEDGMENTS

This research was supported by Army Research Office Award No. W911NF-14-1-0228 (J.Q.), Air Force Office of Scientific Research Grant No. FA9550-15-1-0184 (G.Z.), and Air Force Office of Scientific Research under AFOSR BRI Grant FA9550-12-1-0481 (A.N.A.). This work used the Extreme Science and Engineering Discovery Environment (XSEDE),[30] which is supported by National Science Foundation Grant Number ACI-1053575.

REFERENCES

(1) Fujishima, A.; Honda, K. Electrochemical photolysis of water at a semiconductor electrode. *Nature* **1972**, *238*, 37−38.
(2) Liu, C.; Dasgupta, N. P.; Yang, P. Semiconductor nanowires for artificial photosynthesis. *Chem. Mater.* **2014**, *26*, 415−422.
(3) Frese, K., Jr.; Madou, M.; Morrison, S. Investigation of photoelectrochemical corrosion of semiconductors. *J. Phys. Chem.* **1980**, *84*, 3172−3178.
(4) Chen, Y. W.; Prange, J. D.; Dühnen, S.; Park, Y.; Gunji, M.; Chidsey, C. E.; McIntyre, P. C. Atomic layer-deposited tunnel oxide stabilizes silicon photoanodes for water oxidation. *Nat. Mater.* **2011**, *10*, 539−544.
(5) Hu, S.; Shaner, M. R.; Beardslee, J. A.; Lichterman, M.; Brunschwig, B. S.; Lewis, N. S. Amorphous TiO_2 coatings stabilize Si, GaAs, and GaP photoanodes for efficient water oxidation. *Science* **2014**, *344*, 1005−1009.
(6) Lee, M. H.; Takei, K.; Zhang, J.; Kapadia, R.; Zheng, M.; Chen, Y. Z.; Nah, J.; Matthews, T. S.; Chueh, Y. L.; Ager, J. W.; Javey, A. p-Type InP Nanopillar Photocathodes for Efficient Sola-Driven Hydrogen Production. *Angew. Chem.* **2012**, *124*, 10918−10922.
(7) Hettick, M.; Zheng, M.; Lin, Y. J.; Sutter-Fella, C. M.; Ager, J. W.; Javey, A. Nonepitaxial Thin-Film InP for Scalable and Efficient Photocathodes. *J. Phys. Chem. Lett.* **2015**, *6*, 2177−2182.
(8) Qiu, J.; Zeng, G.; Pavaskar, P.; Li, Z.; Cronin, S. B. Plasmon-enhanced water splitting on TiO_2-passivated GaP photocatalysts. *Phys. Chem. Chem. Phys.* **2014**, *16*, 3115−3121.
(9) Zeng, G.; Qiu, J.; Li, Z.; Pavaskar, P.; Cronin, S. B. CO_2 Reduction to Methanol on TiO_2-Passivated GaP Photocatalysts. *ACS Catal.* **2014**, *4*, 3512−3516.
(10) Zeng, G.; Qiu, J.; Hou, B.; Shi, H.; Lin, Y.; Hettick, M.; Javey, A.; Cronin, S. B. Enhanced Photocatalytic Reduction of CO_2 to CO through TiO_2 Passivation of InP in Ionic Liquids. *Chem. - Eur. J.* **2015**, *21*, 13502−13507.
(11) Lin, Y.; Kapadia, R.; Yang, J.; Zheng, M.; Chen, K.; Hettick, M.; Yin, X.; Battaglia, C.; Sharp, I. D.; Ager, J. W.; Javey, A. Role of TiO2 Surface Passivation on Improving the Performance of p-InP Photocathodes. *J. Phys. Chem. C* **2015**, *119*, 2308−2313.
(12) Shi, J.; Li, Z.; Kvit, A.; Krylyuk, S.; Davydov, A. V.; Wang, X. Electron Microscopy Observation of TiO_2 Nanocrystal Evolution in High-Temperature Atomic Layer Deposition. *Nano Lett.* **2013**, *13*, 5727−5734.
(13) Viswanathan, V.; Pickrahn, K. L.; Luntz, A. C.; Bent, S. F.; Norskov, J. K. Nanoscale Limitations in Metal Oxide Electrocatalysts for Oxygen Evolution. *Nano Lett.* **2014**, *14*, 5853−5857.
(14) Pham, H. H.; Wang, L. W. Electronic structures and current conductivities of B, C, N and F defects in amorphous titanium dioxide. *Phys. Chem. Chem. Phys.* **2015**, *17*, 11908−11913.
(15) Pan, J. M.; Maschhoff, B.; Diebold, U.; Madey, T. Interaction of water, oxygen, and hydrogen with TiO_2 (110) surfaces having different defect densities. *J. Vac. Sci. Technol., A* **1992**, *10*, 2470−2476.
(16) Lu, G.; Linsebigler, A.; Yates, J. T., Jr. Ti^{3+} defect sites on TiO_2 (110): production and chemical detection of active sites. *J. Phys. Chem.* **1994**, *98* (45), 11733−11738.
(17) Lindan, P.; Harrison, N.; Gillan, M.; White, J. First-principles spin-polarized calculations on the reduced and reconstructed TiO_2 (110) surface. *Phys. Rev. B: Condens. Matter Mater. Phys.* **1997**, *55*, 15919.
(18) Krüger, P.; Bourgeois, S.; Domenichini, B.; Magnan, H.; Chandesris, D.; Le Fevre, P.; Flank, A.; Jupille, J.; Floreano, L.; Cossaro, A.; et al. Defect states at the TiO_2 (110) surface probed by resonant photoelectron diffraction. *Phys. Rev. Lett.* **2008**, *100*, 055501.
(19) Von Oertzen, G.; Gerson, A. O deficiency in the rutile TiO_2 (110) surface: Ab initio quantum chemical investigation of the electronic properties. *Int. J. Quantum Chem.* **2006**, *106*, 2054−2064.
(20) Qiu, J.; Zeng, G.; Ha, M.-A.; Ge, M.; Lin, Y.; Hettick, M.; Hou, B.; Alexandrova, A. N.; Javey, A.; Cronin, S. B. Artificial Photosynthesis on TiO2-Passivated InP Nanopillars. *Nano Lett.* **2015**, *15*, 6177−6181.
(21) Giannozzi, P.; Baroni, S.; Bonini, N.; Calandra, M.; Car, R.; Cavazzoni, C.; Ceresoli, D.; Chiarotti, G. L.; Cococcioni, M.; Dabo, I.; et al. QUANTUM ESPRESSO: a modular and open-source software project for quantum simulations of materials. *J. Phys.: Condens. Matter* **2009**, *21*, 395502.
(22) Kohn, W.; Sham, L. J. Self-consistent equations including exchange and correlation effects. *Phys. Rev.* **1965**, *140*, A1133.
(23) Lee, C.; Yang, W.; Parr, R. G. Development of the Colle-Salvetti correlation-energy formula into a functional of the electron density. *Phys. Rev. B: Condens. Matter Mater. Phys.* **1988**, *37*, 785.
(24) Burke, K.; Werschnik, J.; Gross, E. Time-dependent density functional theory: Past, present, and future. *J. Chem. Phys.* **2005**, *123*, 062206.
(25) Perdew, J. P.; Burke, K.; Ernzerhof, M. Generalized gradient approximation made simple. *Phys. Rev. Lett.* **1996**, *77*, 3865.
(26) Grimme, S.; Antony, J.; Ehrlich, S.; Krieg, H. A consistent and accurate ab initio parametrization of density functional dispersion correction (DFT-D) for the 94 elements H-Pu. *J. Chem. Phys.* **2010**, *132*, 154104.
(27) Tilocca, A.; Selloni, A. Structure and reactivity of water layers on defect-free and defective anatase TiO_2 (101) surfaces. *J. Phys. Chem. B* **2004**, *108*, 4743−4751.
(28) Tilocca, A.; Selloni, A. Reaction pathway and free energy barrier for defect-induced water dissociation on the (101) surface of TiO_2-anatase. *J. Chem. Phys.* **2003**, *119*, 7445−7450.
(29) Fujimori, Y.; Kaden, W. E.; Brown, M. A.; Roldan Cuenya, B.; Sterrer, M.; Freund, H.-J. Hydrogen Evolution from Metal−Surface Hydroxyl Interaction. *J. Phys. Chem. C* **2014**, *118*, 17717−17723.
(30) Towns, J.; Cockerill, T.; Dahan, M.; Foster, I.; Gaither, K.; Grimshaw, A.; Hazlewood, V.; Lathrop, S.; Lifka, D.; Peterson, G. D.; et al. XSEDE: accelerating scientific discovery. *Comput. Sci. Eng.* **2014**, *16*, 62−74.

DOI: 10.1021/acs.chemmater.5b03246
Chem. Mater. 2015, 27, 7977−7981